Research Article | Vol. 6, No. 7 | 1 Jul 2016 | OPTICAL MATERIALS EXPRESS 2404

Optical Materials EXPRESS

Theoretical analysis and experiment on Eu reduction in alumina optical materials

YAN YANG,[1] BU WANG,[1] ALASTAIR CORMACK,[1] EUGENIUSZ ZYCH,[2] HYO JIN SEO,[3] AND YIQUAN WU[1,*]

[1]*Kazuo Inamori School of Engineering, New York State College of Ceramics, Alfred University, Alfred, New York, 14802, USA*
[2]*Faculty of Chemistry, University of Wroclaw, 50-383 Wroclaw, Poland*
[3]*Department of Physics, Pukyong National University, Busan 608-737, South Korea*
**wuy@alfred.edu*

Abstract: Density functional theory simulation with a U correction (DFT + U) was adopted to predict the proper experimental conditions required to generate divalent europium (Eu^{2+}) in α-Al_2O_3 host material consolidated via vacuum consolidation. Accordingly, samples of 0.1 at% Eu^{2+}:α-Al_2O_3 were obtained by gelcasting, followed by high vacuum sintering process (<10^{-3} Pa). The room temperature photoluminescence excitation and emission spectra of this composition were examined and characteristic broad band positioned in the blue part of spectrum was detected under UV excitation. This luminescence decay trace had two-exponential character and the average decay time of 0.1 at% Eu^{2+}:α-Al_2O_3 was 0.080ms.

OCIS codes: (160.2540) Fluorescent and luminescent materials; (160.1890) Detector materials; (160.2220) Defect-center materials; (160.4670) Optical materials.

References and links

1. G. Blasse and A. Bril, "Fluorescence of Eu^{2+} activated alkaline-earth aluminates," Philips Res. Rep. **23**, 201–206 (1968).
2. Y. C. Chiu, W. R. Liu, C. K. Chang, C. C. Liao, Y. T. Yeh, S. M. Jang, and T. M. Chen, "Ca_2PO_4Cl: Eu^{2+}: an intense near-ultraviolet converting blue phosphor for white light-emitting diodes," J. Mater. Chem. **20**(9), 1755–1758 (2010).
3. K. B. Kim, Y. I. Kim, H. G. Chun, T. Y. Cho, J. S. Jung, and J. G. Kang, "Structural and optical properties of $BaMgAl_{10}O_{17}$: Eu^{2+} phosphor," Chem. Mater. **14**(12), 5045–5052 (2002).
4. E. Bayer and G. Schaack, "Two-photon absorption of CaF_2:Eu^{2+}," Phys. Status Solidi **41**(2), 827–835 (1970) (b).
5. G. Patton, F. Moretti, A. Belsky, K. Al Saghir, S. Chenu, G. Matzen, M. Allix, and C. Dujardin, "Light yield sensitization by X-ray irradiation of the $BaAl_4O_7$:$Eu^{(2+)}$ceramic scintillator obtained by full crystallization of glass," Phys. Chem. Chem. Phys. **16**(45), 24824–24829 (2014) (pp.).
6. Y. Wu, L. A. Boatner, A. C. Lindsey, M. Zhuravleva, S. Jones, J. D. Auxier II, H. L. Hall, and C. L. Melcher, "Defect Engineering in SrI_2:Eu^{2+} Single Crystal Scintillators," Cryst. Growth Des. **15**(8), 3929–3938 (2015).
7. M. S. Alekhin, J. T. de Haas, K. W. Kramer, I. V. Khodyuk, L. de Vries, and P. Dorenbos, "Scintillation properties and self-absorption in SrI_2: Eu^{2+}," in Nuclear Science Symposium Conference Record (NSS/MIC) (IEEE, 2010), pp. 1589–1599.
8. N. Cherepy, B. Sturm, O. B. Drury, T. Hurst, S. Sheets, L. Ahle, C. Saw, M. Pearson, S. A. Payne, A. Burger, L. A. Boatner, J. O. Ramey, E. V. van Loef, J. Glodo, R. Hawrami, W. M. Higgins, K. S. Shah, and W. W. Moses, "SrI_2 scintillator for gamma ray spectroscopy," Proc. SPIE **7449**, 74490F (2009).
9. G. A. Appleby, A. Edgar, and G. V. M. Williams, "Structure and photostimulated luminescent properties of Eu-doped M_2BaX_4 (M=Cs, Rb; X=Br, Cl)," J. Appl. Phys. **96**(11), 6281–6285 (2004).
10. G. Gundiah, E. D. Bourret-Courchesne, G. Bizarri, S. M. Hanrahan, A. Chaudhry, A. Canning, W. W. Moses, and S. E. Derenzo, "Scintillation properties of Eu^{2+}-activated barium fluoroiodide," in Nuclear Science Symposium Conference Record (NSS/MIC) (IEEE, 2009), 1575–1578.
11. E. D. Bourret-Courchesne, G. Bizarri, R. Borade, Z. Yan, S. M. Hanrahan, G. Gundiah, A. Chaudhry, A. Canning, and S. E. Derenzo, "Eu^{2+}-doped Ba_2CsI_5, a new high-performance scintillator," Nucl. Instrum. Methods Phys. Res. Sect. A **612**(1), 138–142 (2009).
12. M. Kirm, Y. Chen, S. Neicheva, K. Shimamura, N. Shiran, M. True, and S. Vielhauer, "VUV spectroscopy of Eu doped $LiCaAlF_6$ and $LiSrAlF_6$ crystals," Phys. Status Solidi, C Conf. Crit. Rev. **2**(1), 418–421 (2005).
13. A. Fukabori, "Comparative analysis of scintillation characteristics derived from different emission mechanisms in $BaCl_2$," J. Appl. Phys. **117**(15), 153106 (2015).

#259972 http://dx.doi.org/10.1364/OME.6.002404
Journal © 2016 Received 25 Feb 2016; revised 13 May 2016; accepted 31 May 2016; published 30 Jun 2016

Optical Materials EXPRESS

14. J. Glodo, H. Lingertat, C. Brecher, K. S. Shah, and A. Lempicki, "A new ceramic scintillator for neutron detection: CaF_2: Eu^{2+}/^{6}LiF," in Nuclear Science Symposium Conference Record (NSS/MIC) (IEEE, 2005) **1**, 112–115.
15. M. Sugiyama, T. Yanagida, Y. Fujimoto, Y. Yokota, A. Ito, M. Nikl, T. Goto, and A. Yoshikawa, "Basic study of Eu^{2+}-doped garnet ceramic scintillator produced by spark plasma sintering," Opt. Mater. **35**(2), 222–226 (2012).
16. V. B. Mikhailik, H. Kraus, M. Balcerzyk, W. Czarnacki, M. Moszyński, M. S. Mykhaylyk, and D. Wahl, "Low-temperature spectroscopic and scintillation characterization of Ti-doped Al_2O_3," Nucl. Instrum. Methods Phys. Res, Sect. A **546**, 523–534 (2005).
17. G. Angloher, M. Bruckmayer, C. Bucci, M. Bühler, S. Cooper, C. Cozzini, P. DiStefano, F. Von Feilitzsch, T. Frank, D. Hauff, T. Jagemann, J. Jochum, V. Jörgens, R. Keeling, H. Kraus, M. Loidl, J. Marchese, O. Meier, U. Nagel, F. Pröbst, Y. Ramachers, A. Rulofs, J. Schnagl, W. Seidel, I. Sergeyev, M. Sisti, M. Stark, S. Uchaikin, L. Stodolsky, H. Wulandari, and L. Zerle, "Limits on WIMP dark matter using sapphire cryogenic detectors," Astropart. Phys. **18**(1), 43–55 (2002).
18. C. A. Arguello, D. L. Rousseau, and S. P. S. Porto, "First-order Raman effect in wurtzite-type crystals," Phys. Rev. **181**(3), 1351–1363 (1969).
19. J. L. Bettis, M. H. Whangbo, J. Köhler, A. Bussmann-Holder, and A. R. Bishop, "Lattice dynamical analogies and differences between $SrTiO_3$ and $EuTiO_3$ revealed by phonon-dispersion relations and double-well potentials," Phys. Rev. B **84**(18), 184114 (2011).
20. J. Gegner, T. C. Koethe, H. Wu, Z. Hu, H. Hartmann, T. Lorenz, T. Fickenscher, R. Pöttgen, and L. H. Tjeng, "Electronic structure of RAuMg and RAgMg (R=Eu,Gd,Yb)," Phys. Rev. B **74**(7), 073102 (2006).
21. K. Koga, H. Anno, K. Akai, M. Matsuura, and K. Matsubara, "First-principles study of electronic structure and thermoelectric properties for guest substituted clathrate compounds $Ba_6R_2Au_6Ge_{40}$ (R=Eu or Yb)," Mater. Trans. **48**(8), 2108–2113 (2007).
22. J. P. Allen and G. W. Watson, "Occupation matrix control of d- and f-electron localisations using DFT + U," Phys. Chem. Chem. Phys. **16**(39), 21016–21031 (2014).
23. B. Dorado, B. Amadon, M. Freyss, and M. Bertolus, "DFT+U calculations of the ground state and metastable states of uranium dioxide," Phys. Rev. B **79**(23), 235125 (2009).
24. B. Meredig, A. Thompson, H. A. Hansen, C. Wolverton, and A. van de Walle, "Method for locating low-energy solutions within DFT+U," Phys. Rev. B **82**(19), 195128 (2010).
25. B. Wang, X. N. Xi, and A. N. Cormack, "Chemical Strain and Point Defect Configurations in Reduced Ceria," Chem. Mater. **26**(12), 3687–3692 (2014).
26. H. P. Komsa, T. T. Rantala, and A. Pasquarello, "Finite-size supercell correction schemes for charged defect calculations," Phys. Rev. B **86**(4), 045112 (2012).
27. N. D. M. Hine, K. Frensch, W. M. C. Foulkes, and M. W. Finnis, "Supercell size scaling of density functional theory formation energies of charged defects," Phys. Rev. B **79**(2), 024112 (2009).
28. J. Li, Y. Shi, J. Gong, and G. Chen, "Mössbauer study of amorphous Al_2O_3:Eu^{3+}," J. Mater. Sci. Lett. **16**(9), 743–744 (1997).
29. N. Rakov and G. S. Maciel, "Photoluminescence analysis of α-Al_2O_3 powders doped with Eu^{3+} and Eu^{2+} ions," J. Lumin. **127**(2), 703–706 (2007).
30. M. W. Chase, JANAF thermochemical tables, American Chemical Society and the American Institute of Physics for the National Bureau of Standards, New York, 1985.
31. G. Blasse, W. Wanmaker, J. Ter Vrugt, and A. Bril, "Fluorescence of Eu^{2+} activated alkaline-earth aluminates," Philips Res. Rep **23**, 189–200 (1968).
32. A. Pillonnet, A. Pereira, O. Marty, and C. Champeaux, "Valence state of europium doping ions during pulsed-laser deposition," J. Phys. D Appl. Phys. **44**(37), 375402 (2011).
33. S. Mochizuki, T. Nakanishi, Y. Suzuki, and K. Ishi, "Reversible photoinduced spectral change in Eu_2O_3 at room temperature," Appl. Phys. Lett. **79**(23), 3785–3787 (2001).
34. J. A. Zasadzinski, "A new heat transfer model to predict cooling rates for rapid freezing fixation," J. Microsc. **150**(2), 137–149 (1988).
35. G. Hirata, N. Perea, M. Tejeda, J. A. Gonzalez-Ortega, and J. McKittrick, "Luminescence study in Eu-doped aluminum oxide phosphors," Opt. Mater. **27**(7), 1311–1315 (2005).
36. N. Rakov, G. S. Maciel, W. B. Lozano, and C. B. de Araújoa, "Investigation of Eu^{3+} luminescence intensification in Al_2O_3 powderscodoped with Tb^{3+} and prepared by low-temperature direct combustion synthesis," Appl. Phys. Lett. **88**(8), 081908 (2006).
37. N. Rakov, F. E. Ramos, G. Hirata, and M. Xiao, "Strong photoluminescence and cathodoluminescence due to f-f transitions in Eu^{3+} doped Al_2O_3 powders prepared by direct combustion synthesis and thin films deposited by laser ablation," Appl. Phys. Lett. **83**(2), 272–274 (2003).

1. Introduction

Optical materials based on rare earth activation center, such as neodymium and europium ions, are critical for a wide range of applications including phosphors [1–3], lasers [4], and scintillator materials [5, 6] for ionizing radiation detection [7]. Their optical properties are very sensitive to the host lattice, i.e., crystal field strength, covalency, cation size, etc., and

Optical Materials EXPRESS

therefore considerable attention has been paid to the search for host materials with high performance and reliability. Many of the recently developed hosts are halides [6, 8–14]. They provide high light output and reasonable scintillation decay time, but suffer from sensitivity to moisture and low mechanical strength, which has substantially limited their applications, especially as scintillators. Oxide ceramics, on the other hand, possess high chemical stability and high transparency, and thus can be ideal candidates for the next generation of scintillator materials. For example, it was recently reported that Eu-doped garnet ($Y_3Al_5O_{12}$) scintillators show very promising scintillation properties [15]. The widely available α-Al_2O_3 has also been considered for cryogenic phonon detector designated for the Dark Matter experiment [16, 17]. Indeed, these materials can also provide good mechanical properties, excellent refractory character, high chemical stability and optical transmission over a wide range of wavelengths.

However, efficient identification of high-performance host oxide with proper fabrication conditions is challenging. The chemical state of many rare earth activation centers (i.e., valence) is sensitive to the synthesis condition, and this is coupled with the stringent sintering conditions required to achieve transparency in polycrystalline oxide materials. Predictive method based on computations are also lacking, due to the difficulty in accurately capture the electronic behavior, particularly for the f-electrons, in different atomic environments, at realistically low doping concentration (tenths of a percent), and as a function of experimental conditions. It is therefore no surprise that determining the correct experimental conditions so far has been largely relying on trial and error. In this paper, we present a protocol to use ab-initio simulations based on density functional theory (DFT) to guide the experimental synthesis of rare earth doped transparent polycrystalline ceramics. Using Eu^{2+} doped α-Al_2O_3 as an example, we present the evidence that sophisticated DFT simulations can provide critical guidance for assessing experimental feasibility and selecting effective synthesis conditions. This provides the basis for efficient predictive tools based on computations that would enable high-throughput screening of the similar materials. For validation, Eu:Al_2O_3 ceramics were synthesized by gelcasting techniques and vacuum sintering method with photoluminescence properties and decay time characterized here.

2. Method

2.1 Density functional theory simulations with U correction (DFT + U)

The *ab initio* simulations were performed with VASP, a plane wave DFT package [18]. PBE exchange and correlation functional was used with the plane wave cutoff set to 500 eV. To properly describe the f-electrons of Eu ions, we applied the DFT + U method with an effective U value of 6 eV, according to several previous simulation studies of Eu-containing compounds [19–21]. We paid particular attention to the issues of unphysical sub-orbital occupations raised in recent DFT + U studies, which can lead to incorrect energetics and ionic structures in some materials [22–25]. With a simple scheme proposed recently, which involves ramping the U value iteratively during ionic relaxation [24, 25], we did not find sub-orbital occupations significantly more stable than the ones obtained by the standard method for the systems studied here, although more thorough investigation might be needed.

The target doping concentration of synthesized Eu:Al_2O_3 is 0.1 at. % is well below the dilute solution limit. For example, the probability of a Eu substitution have no other Eu substitution in a nearest neighbor configuration, i.e., all three nearest cation sites around the Eu are occupied by Al ions, is $(99.9\%)^3 = 99.7\%$ in a random distribution. Similarly, in the case of Eu^{2+} compensated with oxygen vacancy, the probability of a Eu dopant in the α-Al_2O_3 lattice (assuming six coordinated, see detailed discussions below) does not have neighboring oxygen vacancy is 99.8%. Therefore, it is necessary to consider the defects as isolated. We note, however, our simulations indeed found considerable association between certain defects, especially in the case of Eu^{2+} and oxygen vacancy (binding energy of 2.5 eV in a 3 × 3 × 1 supercell). Such association would inevitably begin to manifest when the doping concentration increases, and should be taken into consideration in heavily doped cases.

Optical Materials EXPRESS

Within the plane wave DFT frame, the periodic system containing isolated defects must be dealt with care. Especially, charged defects, which are neutralized with electron jellium in the present study, can considerably slow the convergence against system size [26]. To resolve this issue, we adopted a correction scheme proposed by Hine *et al* [27]. In this scheme, a series of supercells of different sizes and shapes containing the same defect are simulated, and the corrected energy is obtained by extrapolating a linear relationship between the energy and the Madelung potential of each supercell (calculated as a function of the defect charge and cell geometry) to infinite system size. For each charged defect in the present study, we fully relaxed four hexagonal corundum supercells (2 × 2 × 1, 2 × 2 × 2, 3 × 3 × 1, 2 × 2 × 3) to extrapolate the corrected defect energy. For Eu^{3+} substitution, no addition charge is involved and the results from 3 × 3 × 1 supercell (270 atoms) are used. For all the structures, relaxation was conducted until forces on all the atoms are below 0.01 eV/Å.

2.2 Synthesis and characterization of Eu: Al_2O_3

0.1 at. % Eu: Al_2O_3 were synthesized by gelcasting technique. Vacuum sintering method were adopted here to provide a cost-effective route to manipulate the valence state of Eu in Eu:Al_2O_3. Eu was introduced in the form of Eu_2O_3 (99.5%, Sigma-Aldrich) and high-purity α-Al_2O_3 powder (>99%) (CR-10, Baikowski, Annecy, France, D_{50} = 0.45 μm) was used as the matrix material. After drying and de-binding of gelled Eu:Al_2O_3, the material is sintered in a vacuum furnace (10^{-3}-10^{-4} Pa) at the temperature 1400-1850 °C for 8 hours with the final sample diameter around 3 mm and thickness in the range of 3-5 mm.

After sintering, the room temperature photoluminescence emission and excitation spectra of Eu: Al_2O_3 were recorded in an apparatus consisting of a Xenon lamp, two grating monochromators and a synchronous light detection system (Fluorolog-Tau-3, Jobin Yvon Inc. Horiba, Japan). The measurements were performed with internal corrections and compensation for the light source. Decay curves were also recorded using a pulsed Nd:YAG laser at 266 nm or 355 nm (Spectron Laser System SL802G, Rugby, UK) with a pulse energy of approximately 5 mJ, 10 Hz repetition rate and 5 ns duration.

3. Results and discussion

3. 1 Density functional theory simulations with U correction (DFT + U) of Eu^{2+}/Eu^{3+}:α-Al_2O_3

We first investigated the defect mechanism for Eu doping in α-Al_2O_3. Mössbauer measurement has indicated that the Eu^{3+} dopant in α-Al_2O_3 has a coordination number of six [28]. There have also been previous work hypothesizing that the Eu^{3+} dopant would substitute Al^{3+}, rather than occupy interstitial sites, based on the bonding covalency and similar X-ray diffraction pattern between pure and doped alumina [28, 29]. In this study, we examined both substitution and interstitial mechanisms. The preferred one was found to be the substitution of Al^{3+} by Eu^{3+} as described by the following defect reaction in Eq. (1):

$$Eu_2O_3 \xrightarrow{Al_2O_3} 2Eu_{Al}^{\times} + 3O_o \quad (1)$$

This should come as no surprise even though both Al^{3+} substitution and octahedral interstitial (tetrahedral interstitial site is too small for large ion such as Eu^{3+}) provide the same coordination environment for Eu^{3+}. The interstitial mechanism places Eu^{3+} adjacent to Al^{3+} ions, causing strong lattice distortions. It also needs to be charge compensated by O^{2-} interstitials or Al^{3+} vacancies, incurring large energetic penalties.

Interestingly, Eu^{2+} dopant also prefers a similar substitution mechanism, even though both substitution and interstitial require other defects (considering the most likely mechanisms: one O^{2-} vacancy per two Eu^{2+} substitutions versus one O^{2-} interstitial per one Eu^{2+} interstitial). The defect reaction equation, describing the reduction of Eu^{3+} to Eu^{2+} in Al_2O_3 host lattice, can therefore be written as Eq. (2):

Optical Materials EXPRESS

$$Eu_2O_3 \xrightarrow{Al_2O_3} 2Eu(2+)'_{Al} + V_O^{\cdot\cdot} + \frac{3}{2}O_2(g) \quad (2)$$

It is worth noting that both isolated Eu^{3+} and Eu^{2+} substations have six-coordinated environments. For both cases, the first coordination shell is well-defined and similar to that of Al^{3+} in Al_2O_3, with two sets of Eu-O bond lengths. It can be seen that, in spite of the substantial size difference between europium and aluminum ions, isolated Eu dopant can be constricted by the host lattice and assume the environment of host cations, at least at a low dopant concentration. This can also apply to other host materials for selecting desired local environment for the luminescence dopant.

As both Eu^{3+} and Eu^{2+} would assume the same lattice site, the reduction reaction of Eu^{3+} to Eu^{2+} can be written as the following Eq. (3), by combining Eq. (1) and (2):

$$Eu_2O_3 \xrightarrow{Al_2O_3} 2Eu(2+)'_{Al} + V_O^{\cdot\cdot} + \frac{3}{2}O_2(g) \quad (3)$$

The reduction enthalpy for this reaction can then be calculated in Eq. (4):

$$E_r = E_{2Eu^{2+}} + E_{V_O^{\cdot\cdot}} + \mu_O(T,P) - E_{2Eu^{3+}} \quad (4)$$

where $(E_{2Eu^{2+}} - E_{2Eu^{3+}})$ is the difference in lattice energy between Eu^{2+} and Eu^{3+} doped structures, and $\mu_O(T,P)$ is calculated as:

$$\mu_O(T,P) = \frac{1}{2}E_{O_2} + \Delta\mu_O^O(T) + k_B T ln(p_{O_2}) \quad (5)$$

where E_{O_2} is the energy of O_2 molecule at 0K, which was calculated from DFT by placing an isolated O_2 molecule in the simulation box. The standard chemical potential of oxygen at higher temperatures can be calculated by correcting E_{O_2} with $\Delta\mu_O^O(T)$, which is obtained from thermodynamic tables [30]. The DFT + U simulations calculated the value of ($E_{2Eu^{2+}} + E_{V_O^{\cdot\cdot}} + \frac{1}{2}E_{O_2} - E_{2Eu^{3+}}$) as 3.50 eV. Using this value, the reduction level can be estimated as a function of oxygen partial pressure according to reaction kinetics theory. Ignoring the vibrational entropy contribution, the temperature-dependence equilibrium constant follows the Boltzmann distribution:

$$\frac{\left[Eu'_{Eu}\right]^2\left[V_O^{\cdot\cdot}\right]}{\left[Eu_{Eu}^{\times}\right]^2\left[O_O^{\times}\right]} = \exp\left(-\frac{E_r}{kT}\right) \quad (6)$$

where $\left[Eu'_{Eu}\right]$, $\left[Eu_{Eu}^{\times}\right]$, $\left[V_O^{\cdot\cdot}\right]$, $\left[O_O^{\times}\right]$ are equilibrium concentrations of Eu^{2+}, Eu^{3+}, oxygen vacancies, and oxygen ions, respectively, and they satisfy:

$$\left[Eu'_{Eu}\right] = 2\left[V_O^{\cdot\cdot}\right] \quad (7)$$

and, considering that $\left[V_O^{\cdot\cdot}\right]+\left[O_O^{\times}\right]$ gives the total concentration of oxygen sites in the host Al_2O_3:

$$\frac{\left[Eu'_{Eu}\right]+\left[Eu_{Eu}^{\times}\right]}{\left[V_O^{\cdot\cdot}\right]+\left[O_O^{\times}\right]} = \frac{\left[Eu'_{Eu}\right]+\left[Eu_{Eu}^{\times}\right]}{\frac{3}{2}\left[Al_{Al}^{\times}\right]} = \frac{2}{3}c_{Eu} \quad (8)$$

where c_{Eu} is the doping concentration of Eu. Solving Eqs. (6), (7) and (8), the Eu^{2+} concentration can be obtained. The results are plotted in Fig. 1. The Eu^{2+} concentration shows a dependence on oxygen partial pressure with a characteristic exponent of −1/6. At high

Optical Materials EXPRESS

oxygen partial pressure, reduction is limited. Typical vacuum furnaces for high temperature sintering can maintain oxygen partial pressure in the range of $0.21 \times (10^{-3}\text{-}10^{-4})$ Pa, which is marked with the dotted lines. It can be seen that, for $p(O_2)$ in this range, a high temperature above 1700℃ can reduce majority (>95%) of the Eu^{3+} to Eu^{2+}. Such a high temperature can also encourage oxygen diffusion so that the reduction equilibrium can be reached efficiently.

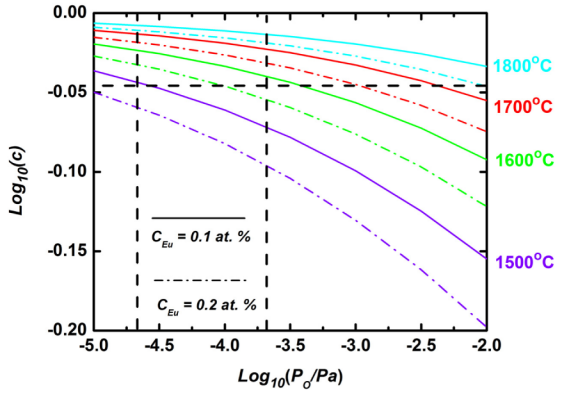

Fig. 1. Calculated Eu^{2+} concentration (in $\log_{10}(c)$, where $c = [Eu^{2+}]/[Eu]$) versus oxygen partial pressure (in $\log_{10}(P_O)$, where P_O is oxygen partial pressure in Pa) in the temperature range between 1400~1900 °C. Vertical dashed lines mark the range of oxygen partial pressure used in vacuum synthesize. The horizontal dashed line indicates c = 95%.

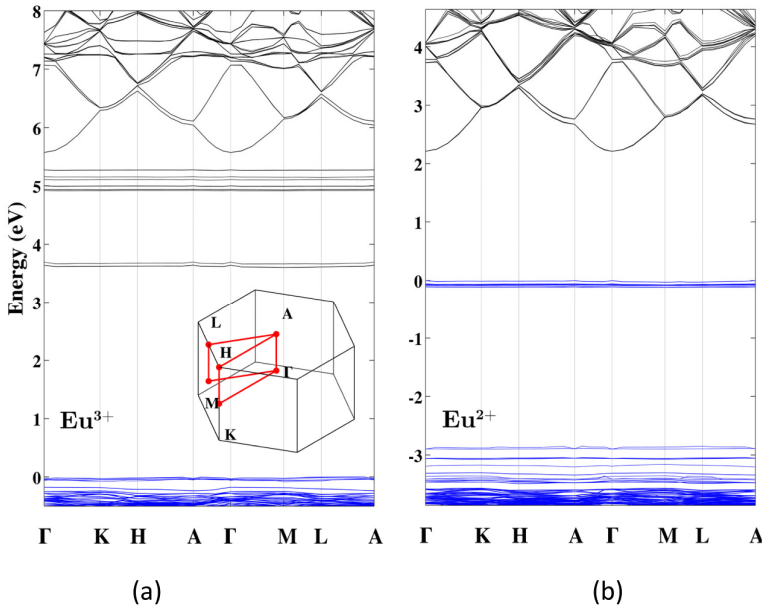

Fig. 2. Band structure of Eu^{3+} (a) and Eu^{2+} (b) doped alumina. The Fermi energy is set to 0 eV. For comparison, the two plots are arranged so that the energy levels contributed mainly by alumina are aligned. For clarity, unoccupied and occupied bands are shown in blue. Spin up and spin down levels are plotted with solid and dotted lines, respectively.

The electronic band structures of Eu^{3+} and Eu^{2+} doped α-Al_2O_3 are also calculated from the DFT + U simulations, as shown in Fig. 2. We observe no substantial differences between the electronic bands contributed by the host material, α-Al_2O_3 between the two cases. The defect states contributed by the dopants in the band gap are well defined, and show no obvious characteristics of the α-Al_2O_3 symmetry. Therefore, we expect the luminescence in

Optical Materials EXPRESS

both cases to retain its characteristic spectrum. However, it is worth noting that the effect of oxygen vacancy, especially the association between the dopant and vacancy, is not considered here. This could potentially cause alterations of the spectrum of the Eu^{2+} doped material, which warrants further investigations.

3.2 Photoluminescence characterization of $Eu^{2+}/Eu^{3+}:Al_2O_3$

3.2.1 Room temperature photoluminescence emission and excitation of $Eu^{2+}/Eu^{3+}:Al_2O_3$

Room temperature photoluminescence excitation and emission spectra of Eu: Al_2O_3 were recorded in Fig. 3 and Fig. 4. The photoluminescence excitation spectrum of Eu^{2+}: Al_2O_3 (Fig. 3) shows two over-lapped excitation peaks with the centers at 277 nm and 330 nm, coming from the emission behavior of Eu^{2+}. The blue emission of Eu:Al_2O_3 comes from the transition of Eu^{2+} between $4f^65d^1$ and $4f^7$ ($^8S_{7/2}$) ($Eu^{2+}(4f^7)+h\nu \rightarrow Eu^{2+*}(4f^65d^1)$). Such f-d transition and broadband emission are usually strongly dependent on the local atomic environment of the activation center. Gaussian fitting analysis of the excitation spectrum of vacuum-sintered Eu^{2+}: Al_2O_3 (monitored at 430 nm, Fig. 3) showed two broad excitation peaks at 277 nm and 330 nm, respectively, indicating that the Eu^{2+} ions are located in low-symmetry sites with a broad crystal field distribution [31] and a large field splitting of 5d band [29]. Such excitation spectrum is different from those measured for Eu^{2+}:Al_2O_3 powder [29] and Eu^{2+}:Al_2O_3 film [32]. It is possible that the fabrication process has led to changes in the local symmetry of the Eu^{2+} activator. As shown by the DFT + U calculations, the Eu^{2+} dopants substitute Al^{3+}, accompanied by oxygen vacancies. The oxygen vacancies may form F^+-centers [33], and contribute to broad excitation and emission spectra in the UV region. Additionally, strong association may exist between dopants and vacancies. Under favorable synthesis conditions, e.g. slow cooling rate, defect clusters such as $Eu(2+)'_{Al}-V_O^{\cdot\cdot}$ may be obtained, which leads to a change in the local symmetry of the Eu^{2+} activator and, consequently, the crystal field felt by Eu^{2+} ions. Indeed, the bulk samples may experience slower cooling in the center than powders and films even when the same nominal cooling rate is used [34]. Other factors, such as phase separation, defect segregation at grain boundary, etc., could also contribute to the changes in the local atomic environment of the activation centers, which warrants further investigations.

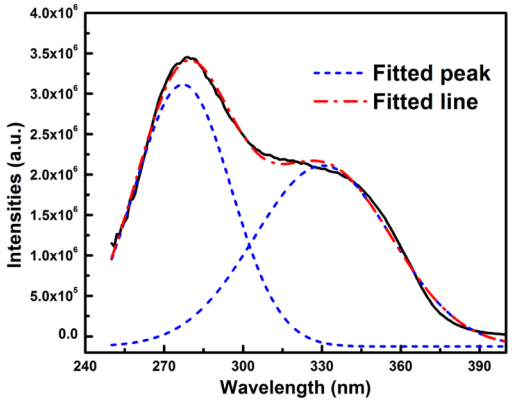

Fig. 3. Room temperature photoluminescence excitation spectra of vacuum-sintered 0.1at% Eu^{2+}: Al_2O_3 monitored at 430 nm with corresponding Gaussian fitting curves.

Air-sintered Eu:Al_2O_3 was also examined under excitation by UV light (277 nm), which showed the characteristic photoluminescence peaks of Eu^{3+} at 588 nm ($^5D_0$-$^7F_1$) and 611 nm ($^5D_0$-$^7F_2$) [35–37]. In comparison, under excitation with UV light (277 nm and 330 nm),

Optical Materials EXPRESS

vacuum sintered Eu:Al_2O_3 only showed one broad peak in the wavelength range of 330-600 nm with a peak center near 430 nm but none of the characteristic peaks of Eu^{3+}. This indicates that the reduction of Eu^{3+} —› Eu^{2+} in the Al_2O_3 host was achieved by vacuum sintering at temperatures of 1750-1850 °C, as predicted by the DFT + U calculations.

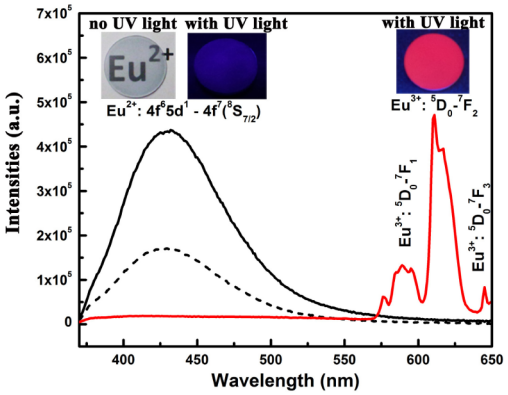

Fig. 4. Room temperature photoluminescence emission spectra of vacuum-sintered 0.1at% Eu^{2+}: Al_2O_3 and air-sintered 0.1at% Eu^{3+}: Al_2O_3 excited with 277 nm and 330 nm (dark line: Eu^{2+}:Al_2O_3; red line: Eu^{3+}:Al_2O_3).

3.2.2 Room temperature photoluminescence emission spectra of Eu: Al_2O_3 sintered at varying vacuum-sintering temperature

To further validate the DFT + U calculations, samples were vacuum sintered at different temperatures using the same procedure. The measured emission spectra were shown in Fig. 5. As expected, the intensity of the characteristic Eu^{3+} photoluminescence peak at 611 nm ($^5D_0$-$^7F_2$) decreases with increasing vacuum sintering temperature. In comparison, the emission intensity of Eu^{2+} in the blue light region increases with higher vacuum sintering temperature. The presence of Eu^{3+} is evident at and below 1700 °C, suggesting the calculated Eu^{2+} concentration may be overestimated, which requires further quantification. Nonetheless, the DFT + U calculations provided adequate guidance for selecting the correct sintering condition. It should also be noted that, low porosity and good sintering quality in the samples, a prerequisite for optical applications that require high transmittance, have been obtained at temperatures above 1700 °C.

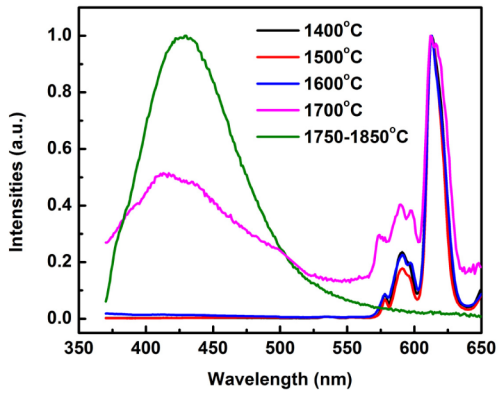

Fig. 5. Photoluminescence spectra of vacuum-sintered 0.1at% Eu^{2+}: Al_2O_3 at room temperature excited with 277 nm as a function of vacuum sintering temperature (normalized to the same height at the spectra maxima).

Optical Materials EXPRESS

3.2.3 Luminescence decay properties of Eu^{2+}:Al_2O_3

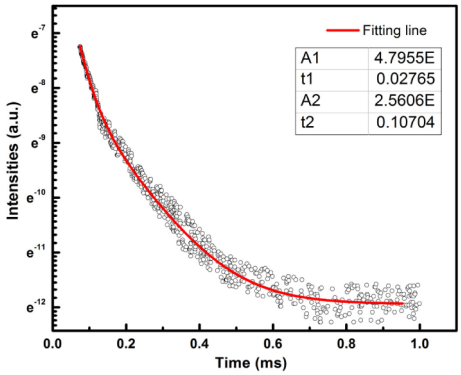

Fig. 6. Decay curve of 0.1at% Eu^{2+}: Al_2O_3 (sintering temperature: 1750°C-1850°C) monitored at 490 nm with the excitation 266 nm at room temperature.

The luminescence decay curve of the vacuum sintered (1750°C-1850°C) 0.1 at. % Eu^{2+}:Al_2O_3 measured at room temperature is shown in Fig. 6, monitored at 490 nm with an excitation wavelength of 266 nm. The luminescence decay curves were fitted by double exponentials ($I = A_1 * exp(-t_1/\tau_2) + A_2 * exp(-t_2/\tau_2)$) with the equation parameter shown in Fig. 6. The decay time of the Eu^{2+} d-f transition is on the order of microseconds. The average decay time of the Eu^{2+} in Al_2O_3 after vacuum-sintering was calculated from the fitting process to be approximately 0.080 ms.

4. Summary

Overall, it can be seen that ab-initio calculations employing an improved DFT + U method for rare earth elements successfully guided the fabrication of Eu in α-Al_2O_3 host. The simulation results showed that Eu^{2+}:Al_2O_3 can be fabricated by gelcasting and a subsequent vacuum sintering process under a vacuum atmosphere of 10^{-3}-10^{-4} Pa in the temperature region of 1750°C-1850 °C. The resultant materials show strong photoluminescence behavior with an average lifetime of 0.080 ms. Additionally, the DFT + U calculations also provided details regarding the lattice distortions and defect associations. The presented method can be easily applied to other rare earth dopants and other host materials.

Funding

Air Force Office of Scientific Research (AFOSR) (FA9550-14-1-0155).